# Synthesis and Characterization of Atomically Flat Methyl-Terminated Ge(111) Surfaces

Keith T. Wong,[†] Youn-Geun Kim,[‡] Manuel P. Soriaga,[‡] Bruce S. Brunschwig,[‡,§] and Nathan S. Lewis*,[†,‡,§,‖]

[†]Division of Chemistry and Chemical Engineering, [‡]Joint Center for Artificial Photosynthesis, [§]Beckman Institute, and [‖]Kavli Nanoscience Institute, California Institute of Technology, Pasadena, California 91125, United States

S Supporting Information

ABSTRACT: Atomically flat, terraced H−Ge(111) was prepared by annealing in $H_2(g)$ at 850 °C. The formation of monohydride Ge−H bonds oriented normal to the surface was indicated by angle-dependent Fourier-transform infrared (FTIR) spectroscopy. Subsequent reaction in $CCl_3Br(l)$ formed Br-terminated Ge(111), as shown by the disappearance of the Ge−H absorption in the FTIR spectra concomitant with the appearance of Br photoelectron peaks in X-ray photoelectron (XP) spectra. The Br−Ge(111) surface was methylated by reaction with $(CH_3)_2Mg$. These surfaces exhibited a peak at 568 cm^{-1} in the high-resolution electron energy loss spectrum, consistent with the formation of a Ge−C bond. The absorption peaks in the FTIR spectra assigned to methyl "umbrella" and rocking modes were dependent on the angle of the incident light, indicating that the methyl groups were bonded directly atop surface Ge atoms. Atomic-force micrographs of CH_3−Ge(111) surfaces indicated that the surface remained atomically flat after methylation. Electrochemical scanning−tunneling microscopy showed well-ordered methyl groups that covered nearly all of the surface. Low-energy electron diffraction images showed sharp, bright diffraction spots with a 3-fold symmetry, indicating a high degree of order with no evidence of surface reconstruction. A C 1s peak at 284.1 eV was observed in the XP spectra, consistent with the formation of a C−Ge bond. Annealing in ultrahigh vacuum revealed a thermal stability limit of ~400 °C of the surficial CH_3−Ge(111) groups. CH_3−Ge(111) surfaces showed significantly greater resistance to oxidation in air than H−Ge(111) surfaces.
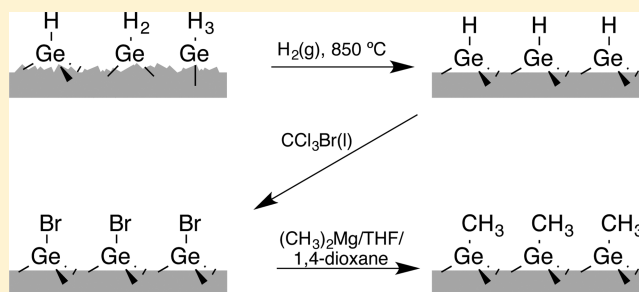
INTRODUCTION

Although the first transistor was made on a Ge crystal, the dominant substrate for semiconductor electronics eventually became Si, owing largely to the ease with which a Si/SiO_2 interface of high electronic quality can be formed. However, as device sizes continually shrink, high leakage current has required the SiO_2 gate dielectric to be replaced by high-κ dielectrics. The move to high-κ dielectrics removes one of the primary reasons—the high defect density at the Ge/GeO_x interface—that Ge has not been frequently used in semiconductor devices, and thus, its use opens the door to take advantage of the high hole mobility of Ge.[1−3] Moreover, the 0.67 eV band gap of Ge is well suited to the absorption of infrared radiation, and Ge or SiGe alloys are frequently used as rear absorbers in multijunction solar cells.[4,5] Applications for Ge in solar cells or in semiconductor electronics require a stable, low defect-density surface, which cannot be achieved by oxidation.[6]

Methyl-terminated Ge(111) surfaces[7,8] have been prepared in a similar manner to that used to alkylate Si(111),[9] specifically through the use of a two-step halogen/alkylation process. Methyl termination of Ge(111) was demonstrated by X-ray photoelectron spectroscopy (XPS) and Fourier-transform

infrared (FTIR) spectroscopy, and surface recombination velocities of <100 cm s^{-1} were observed. However, unlike Si(111), which can be anisotropically etched in $NH_4F(aq)$, no anisotropic etch of the Ge(111) surface has been identified to date. Thus, CH_3−Ge(111) surfaces prepared by wet etching and halogenation/alkylation are expected to be atomically rough. Improvement in the chemical and electrical passivation of Ge(111) may be obtained by the preparation of highly ordered, atomically flat CH_3−Ge(111) surfaces. We describe herein a combination of annealing and a two-step halogenation/alkylation procedure that results in atomically flat CH_3−Ge(111) surfaces. The chemical composition, thermal stability, resistance to oxidation in air, surface topography, and ordering of such surfaces have been characterized by FTIR spectroscopy, high-resolution electron-energy loss spectroscopy (HREELS), XPS, atomic-force microscopy (AFM), electrochemical scanning-tunneling microscopy (EC-STM), and low-energy electron diffraction (LEED).

■ EXPERIMENTAL SECTION

A. Materials. Unless otherwise noted, chemicals were obtained from Sigma-Aldrich or Fisher Scientific and were used as received. Water was obtained from a Barnstead E-Pure water purification system and had a resistivity of 18.2 MΩ cm. Solutions of 10% HF(aq) were prepared by diluting 48 wt % HF(aq) (Transene). Dimethylmagnesium $((CH_3)_2Mg)$ was prepared by addition of small amounts of 1,4-dioxane to 1.0 M methylmagnesium chloride in tetrahydrofuran (THF) (diluted from 3.0 M CH_3MgCl) until the $MgCl_2$·dioxane complex ceased to precipitate. The precipitate was then removed by passing the solution several times through baked glass wool.

Undoped, n-type Ge wafers (MTI Corp.) that were polished on both sides and oriented within ±0.5° of the (111) crystal plane were cut into the desired size using a diamond scribe. The samples had a resistivity of >50 Ω cm. Ge(111) wafers with a miscut angle of ±0.1° (El-Cat Inc., undoped, double-side polished, ρ > 30 Ω cm) were used for AFM imaging.

B. Surface Modification. Immediately prior to surface modification, samples were cleaned by rinsing sequentially with water, methanol, acetone, methanol, and water, followed by 5 min of sonication in acetone and then by 5 min of sonication in methanol. The samples were subsequently repeatedly dipped in 10% HF(aq) for 1 min and in 30% H_2O_2(aq) for 1 min, with a water rinse between the steps. After three cycles of etching and oxidation, the samples were immersed in 10% HF (aq) for 1 min, rinsed with water, and dried under a stream of Ar(g).

Cleaned Ge samples were loaded into a tube furnace that was repeatedly purged with He(g) and pumped out before being pumped down to <0.5 mTorr. Hydrogen-termination of the Ge samples was achieved by annealing the cleaned Ge surfaces at 850 °C for 15 min under 1 atm of H_2(g) at a flow rate of 500 SCCM (standard cubic centimeters at STP). Samples were cooled to <100 °C under H_2(g) and were immediately transferred into an N_2(g)-purged flushbox upon removal from the tube furnace.

H-terminated Ge(111) surfaces were rinsed with anhydrous THF, and they were brominated in neat CCl_3Br for 1 min at 50 °C, with several grains of benzoyl peroxide added as a radical initiator. The samples were rinsed with anhydrous THF following bromination. The Br−Ge(111) surfaces were methylated for 12−16.5 h at 50 °C in $(CH_3)_2Mg$/THF/1,4-dioxane. Methylated surfaces were then rinsed thoroughly with anhydrous THF; removed from the N_2(g)-purged flushbox; sequentially sonicated for 10 min in THF, methanol, and water; and dried under a stream of Ar(g).

C. Characterization. *1. FTIR Spectroscopy.* IR spectra were collected using a Thermo Scientific Nicolet 6700 FTIR spectrometer equipped with a thermoelectrically cooled deuterated triglycine sulfate (DTGS) detector and a dry N_2(g) purge. Spectra were collected in transmission mode with the wafer oriented such that the angle between the surface normal and incident light beam was either 74° or 30°. The reported spectra represent averages of 1000 scans with 4 cm^{-1} resolution, collected after at least 25 min of purging the chamber following loading of the sample.

2. X-ray Photoelectron Spectroscopy. XP spectra were collected using a Kratos AXIS Ultra DLD spectrometer equipped with a magnetic immersion lens that consisted of a spherical mirror and concentric hemispherical analyzers with a delay-line detector (DLD). A monochromatic Al Kα source (1486 eV) was used for X-ray excitation, and ejected electrons were collected normal to the surface. The analysis chamber was maintained at <5 × 10^{-9} Torr. All XPS energies are reported as binding energies in eV.

To identify the elements present on the surface, survey scans from 0 to 1200 eV were collected at a pass energy of 80 eV. High-resolution scans were collected at a pass energy of 10 eV for the Ge 3d (25−37 eV), C 1s (280−292 eV), and Br 3d (64−76 eV) photoelectron regions.

As necessary, sample heating was performed in the XPS analysis chamber. The sample was held to a Mo disc (5 mm diameter ×1 mm) by a stainless steel clip. The disc was suspended between two W wires through which current was passed to heat the sample. The sample

temperature was measured by an E-type (chromel−constantan) thermocouple that was spot-welded to the back side of the Mo disc. Feedback control of the temperature was provided by a Eurotherm controller. Temperature ramp rates no greater than 1 °C s^{-1} were used. The temperature was held constant for 60 min once the desired temperature had been reached and the sample was then cooled to ambient temperature for analysis by XPS.

3. High-Resolution Electron-Energy Loss Spectroscopy. HREELS data were obtained using an LK Technologies ELS5000MCA electron-energy loss spectrometer equipped with a multichannel electron-energy analyzer. The HREELS and LEED spectrometers were attached via a transfer arm to the Kratos XPS system described above, enabling transfer under ultrahigh vacuum (UHV) among all three systems. HREELS spectra were collected with a 5 eV electron-beam energy in a specular geometry, with the monochromator exit and analyzer entrance both positioned 55° from the surface plane. Collection times of at least 300 s were used, and the pressure in the analysis chamber was <1 × 10^{-9} Torr while data were collected.

4. Low-Energy Electron Diffraction. LEED patterns were recorded using an LK technologies RVL2000 reverse-view LEED system. Patterns were collected using a 3.05 A filament current, a 3.0 kV screen voltage, and a 100 V retarding voltage at the specified electron-beam energies. The analysis chamber was maintained below 2 × 10^{-9} Torr during operation of the LEED instrumentation. A Canon EOS Rebel Tli (f/8, 10 s exposure, ISO400) camera was used to record the LEED patterns.

5. Atomic-Force Microscopy. Atomic-force micrographs were recorded using a Bruker MultiMode 8 AFM with a Bruker Nanoscope V controller. Bruker TESPA and TESPA-V2 probes were used in tapping mode. Data were recorded and processed using Bruker Nanoscope 8.15 and Nanoscope Analysis 1.50 software, respectively. Postcollection data processing was limited to image flattening to remove the background tilt and bow. A diamond scribe was used to cut double-side polished, undoped Ge wafers (El-Cat Inc.) oriented within ±0.1° of the (111) crystal plane into the desired size for AFM. The samples had a resistivity of >30 Ω cm.

6. Electrochemical Scanning-Tunneling Microscopy. EC-STM images were obtained using a Nanoscope E (Digital Instruments, Veeco) STM with a three-electrode potentiostat. An electrochemical cell was custom-crafted from Kel-F (Emco Industrial Plastics, Inc.) and fitted with a Pt counter and a Pt pseudoreference electrode calibrated against a Ag/AgCl reference cell. W tips were electrochemically etched (15 V AC in 1.0 M KOH(aq)) from 0.25 mm diameter W wires. Experiments were performed in constant-current mode under potential control at the measured at open-circuit potential (−0.2 V vs Ag/AgCl) with the Ge surface immersed in 0.10 M $HClO_4$(aq).

D. Data Analysis. XPS data were analyzed using CasaXPS v2.3.16 software. High-resolution scans were fit using a Shirley (Ge 3d, C 1s) or offset Shirley (Br 3d) background. Gaussian/Lorentzian product lineshapes were used with a 30% Lorentzian component except for the bulk Ge $3d_{5/2}$ and $3d_{3/2}$ peaks, which were fit with an asymmetric Gaussian/Lorentzian convolution that accounted for the inherent asymmetry due to surface states.

The methods used for quantitative analysis of the XPS data are based on those described previously.[10] The fractional monolayer coverage of Br or hydrocarbon overlayers, Φ_{ov}, was obtained using the relationship:

$$\Phi_{ov} = \frac{N_{ov}}{N_{sites}} = \frac{(\lambda \sin \theta)}{N_{sites}} \left(\frac{SF_{Ge}}{SF_{ov}} \right) \left(\frac{I_{ov}}{I_{Ge}} \right) \rho_{Ge} \qquad (1)$$

where λ is the photoelectron escape depth (assumed to be approximately equal for Ge and the overlayer), θ is the photoelectron takeoff angle measured from the plane of the surface, N_{sites} is the areal density of surface sites on the Ge(111) surface, SF is the modified sensitivity factor, ρ_{Ge} is the atomic density of Ge, and I is the peak intensity. The photoelectron escape depth was taken to be 3.5 nm,[11] the atomic density of Ge was taken to be 4.42 × 10^{22} cm^{-3},[7] and the areal density of the Ge(111) surface was taken to be 7.22 × 10^{14} cm^{-2}.

Modified sensitivity factors, SF_x, accounting for the energy dependence of the electron escape depth, were calculated using

$$SF_x = SF\left(\frac{1486 - BE}{1486 - 284}\right)^{S_{exp}} \quad (2)$$

where SF is the transmission-corrected sensitivity factor obtained from the appropriate Kratos relative sensitivity factor library, BE is the electron binding energy in eV, and S_{exp} is the sensitivity exponent, taken to be 0.69 for our system.

For comparison, the coverage of methyl groups on $CH_3-Ge(111)$ surfaces was also calculated by comparison to the XPS data obtained on $CH_3-Si(111)$ surfaces. Proper preparation of $CH_3-Si(111)$ surfaces has been shown by synchrotron XPS,[12] low-temperature scanning-tunneling microscopy,[13,14] and helium-atom scattering[15] to produce surfaces with near 100% coverage of surface Si atoms, a high degree of long-range ordering, and a low defect density. Therefore, the $CH_3-Si(111)$ surface served as an excellent standard for estimating the overlayer coverage of the $CH_3-Ge(111)$ surfaces. The coverage of a $CH_3-Ge(111)$ surface was accordingly also calculated using the relationship:

$$\Phi_{ov} = \frac{\left[I_C\left(\frac{SF_{Ge}}{I_{Ge}}\right)\right]_{CH_3-Ge(111)}}{\left[I_C\left(\frac{SF_{Si}}{I_{Si}}\right)\right]_{CH_3-Si(111)}}\left(\frac{\sigma_{Si}}{Ge}\right) \quad (3)$$

where σ_{Si} and σ_{Ge} represent the surface atomic densities of the Si(111) and Ge(111) surfaces—7.83×10^{14} and 7.22×10^{14} cm^{-2}, respectively. Although this method relies on the relative accuracy of the sensitivity factors of SF_{Si} and SF_{Ge}, the substrate-overlayer model of eq 1 also relies on the accuracy of λ, SF_{Ge}, and SF_C.

The methods used to calculate the thickness and coverage of oxidized Ge have also been described previously.[11] The thickness, d, of oxidized Ge was calculated using the formula:

$$d = \lambda_{ov}\sin\theta\left(\ln\left[1 + \left(\frac{I_{Ge}^{\circ}}{I_{ov}^{\circ}}\right)\right]\right) \quad (4)$$

where λ_{ov} is the photoelectron escape depth through the oxide overlayer, taken to be 3.0 nm for Ge 3d photoelectrons,[16] and $I_{Ge}^{\circ}/I_{ov}^{\circ}$ is an experimentally determined normalization factor based on the intensity ratio of the signal for pure Ge relative to the signal for pure Ge oxide, and was taken to have a value of 1.51.[11] The coverage was then calculated assuming a value of 0.32 nm for the thickness of a monolayer of GeO_2.[17]

■ RESULTS

A. Vibrational Spectroscopy. Figure 1 shows transmission FTIR spectra at two different angles of incident light for a H−Ge(111) surface that was formed by annealing at 850 °C under $H_2(g)$. Table 1 presents the observed peaks, their primary polarization directions, and the peak assignments for such surfaces. The sharp vibrational modes at 1975 and 563 cm^{-1} were assigned to the monohydride Ge−H stretching (ν(Ge−H)) and bending (δ(Ge−H)) modes, respectively.[18,19] Fitting the ν(Ge−H) and δ(Ge−H) peaks with Gaussian lineshapes yielded a full width at half-maximum of 3.1 and 3.2 cm^{-1}, respectively, establishing an upper limit to the actual line width due to the instrument-limited 4 cm^{-1} resolution at which the spectra were collected. The ν(Ge−H) and δ(Ge−H) modes both showed strong signals at an incident light angle of 74° off the surface normal, whereas at an angle of 30° the ν(Ge−H) mode was very weak while the δ(Ge−H) mode absorbed strongly. At a 74° incident angle, significantly more light polarized perpendicular to the surface is transmitted then light polarized parallel to the surface, while at 30° the opposite
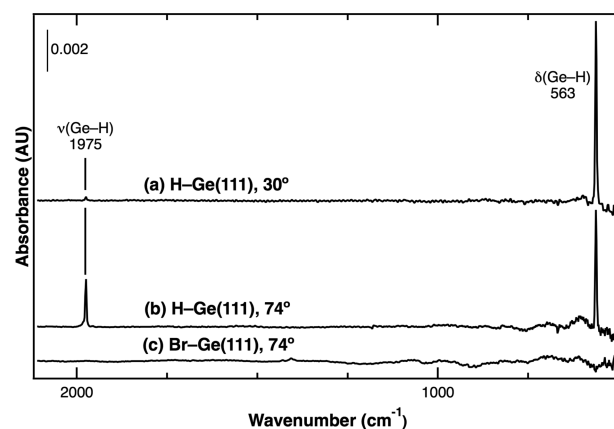

Figure 1. Transmission FTIR spectra of (a) an H−Ge(111) surface at a 30° incident angle, (b) an H−Ge(111) surface at a 74° incident angle, and (c) a Br−Ge(111) surface at a 74° incident angle. The background sample for all of these spectra was an HF-etched Ge(111) surface that had been exposed to ambient air. The incident angle is given as the angle between the surface normal of the sample and the excitation beam.

Table 1. Position, Primary Polarization Direction, and Assignment of H−Ge(111) and CH_3−Ge(111) Vibrational Modes Observed by FTIR Spectroscopy and HREELS

FTIR spectroscopy		HREELS	
position (cm^{-1})	primary polarization direction	position (cm^{-1})	assignment
		H−Ge(111)	
1975	z	n/a	Ge−H stretch mode
563	∥	n/a	Ge−H bend mode
		CH_3−Ge(111)	
2956	∥	2910	C−H stretching mode
2928	z	2910	C−H stretching mode
2906	z	2910	C−H stretching mode
2860	∥	2910	C−H stretching mode
-	-	1411	asymmetric C−H deformation mode
1234	z	1234	symmetric C−H deformation mode (CH_3 umbrella mode)
762	∥	780	CH_3 rocking mode
-	-	568	Ge−C stretching mode

situation occurs. Accordingly, the relative intensities of vibrational modes perpendicular to the surface should increase in intensity as the incident angle is increased, whereas modes oriented parallel to the surface should exhibit a decrease in intensity. Thus, the data were consistent with the ν(Ge−H) mode being polarized perpendicular to the surface and with the δ(Ge−H) mode being polarized parallel to the surface. No absorbance characteristic of Ge−H stretching associated with GeH_2 and GeH_3 species was observed in the 2000−2100 cm^{-1} region.[18,19]

Figure 1 also displays the transmission FTIR spectrum of a Br−Ge(111) surface that was formed by reaction of a H−Ge(111) surface with $CCl_3Br(l)$. No absorbance was observed at the frequencies that corresponded to ν(Ge−H) and δ(Ge−H) vibrational modes, indicating complete removal of Ge−H species from the surface. The Ge−Br stretching and deformation modes were expected to occur at frequencies too low to be detected by our experimental apparatus.

Figure 2 presents the transmission FTIR spectra of a CH_3–Ge(111) surface formed by the reaction of Br–Ge(111) with

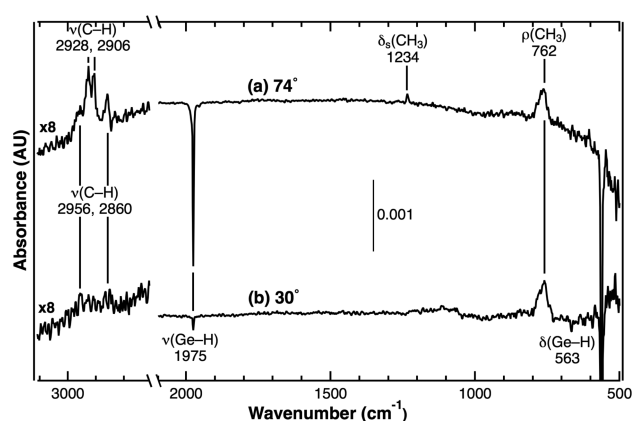**Figure 2.** Transmission FTIR spectra of a CH_3–Ge(111) collected with the surface normal oriented at an angle of (a) 74° or (b) 30° relative to the incident excitation beam. Both spectra used a H–Ge(111) surface as a background, and the absorbance in the 2700–3100 cm^{-1} region was magnified 8-fold for clarity of presentation.

Figure 3. HREELS data for a CH_3–Ge(111) surface (a) as-prepared and (b) after a 60 min anneal at 350 °C. The region above 150 cm^{-1} energy loss has been magnified 20-fold for clarity.

$(CH_3)_2Mg/THF/1,4$-dioxane and collected using light incident at two different angles. The peak positions, polarization directions, and assignments are also shown in Table 1. At a 74° incident light angle, positive peaks were observed at 2956, 2928, 2906, and 2860 cm^{-1}, and were assigned to the C–H stretching modes ($\nu(C–H)$) of both the methyl surface functionalization as well as to adventitious hydrocarbon species. The positive peaks at 1234 and 762 cm^{-1} were assigned to the symmetric CH_3 deformation (methyl "umbrella" mode, $\delta_s(CH_3)$) and the CH_3 rocking mode ($\rho(CH_3)$), respectively, as previously reported.[8] The negative peaks observed at 1975 and 563 cm^{-1} corresponded to $\nu(Ge–H)$ and $\delta(Ge–H)$ signals exhibited by the background H–Ge(111) surface. At a 30° incident light angle, the $\delta_s(CH_3)$ mode was not visible above the noise, whereas the $\rho(CH_3)$ mode absorbed strongly. The incident angle dependence indicated that the methyl umbrella and rocking modes were polarized perpendicular and parallel to the surface, respectively, and was consistent with the presence of a Ge–C bond oriented perpendicular to the surface.

Figure 3 shows the HREELS data of a CH_3–Ge(111) surface as prepared and after a 60 min anneal at 350 °C in UHV, respectively. Peak positions and assignments are shown in Table 1. The peaks at 2910, 1234, and 780 cm^{-1} were assigned to the $\nu(C–H)$, $\delta_s(CH_3)$, and $\rho(CH_3)$ vibrational modes, respectively, and were consistent with the transmission FTIR spectra shown in Figure 2. However, the individual C–H stretching modes were not resolved by HREELS. In addition, the HREELS peaks observed at 1411 and 568 cm^{-1} were assigned to the asymmetric CH_3 deformation ($\delta_a(CH_3)$) and to the Ge–C stretching ($\nu(Ge–C)$) modes, respectively. The $\delta_a(CH_3)$ mode was not observed by FTIR spectroscopy, as this mode does not have a significant change in dipole moment and therefore should be IR inactive, whereas IR inactive modes can be observed in HREELS even in a specular geometry.[20] The $\nu(Ge–C)$ mode is expected to be IR active but was not observed by transmission FTIR spectroscopy due to the low absorption cross-section of this mode and the high noise level that was present in the low-wavenumber region for the particular IR instrument used. Small peaks at 921 and 1045
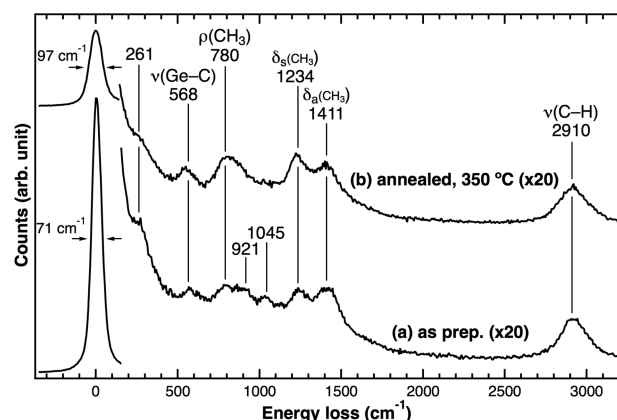
cm^{-1}, and a shoulder on the elastic peak at 261 cm^{-1}, were also observed in the HREELS data of as-prepared CH_3–Ge(111). These peaks were not readily assigned, however, and annealing the surface to 350 °C for 60 min in UHV (Figure 3b) led to the disappearance of the peaks at 921 and 1045 cm^{-1}, suggesting that these signals resulted from physisorbed adventitious species that desorbed upon annealing. No significant change in the peaks assigned to the vibrational modes of the CH_3–Ge(111) surface was observed upon annealing of these samples.

B. X-ray Photoelectron Spectroscopy. Figure 4 displays a representative XP survey spectrum of a CH_3–Ge(111) surface. The spectrum was dominated by Ge photoelectron and Auger lines from the bulk crystal, at Ge 3d (30 eV), Ge 3p (122 eV), Ge 3s (181 eV), Ge LMM (300–600 eV), and by associated plasmon loss peaks. C 1s and O 1s photoelectron peaks were also observed at 285 and 533 eV, respectively, consistent with the presence of surface-bound methyl groups, adventitious hydrocarbons, and/or oxygen-containing adventitious hydrocarbons. No other elements were detected in the survey spectrum, and no Mg from the $(CH_3)_2Mg$ was detected in high-resolution XPS scans (see Supporting Information). Survey spectra of H–Ge(111) and Br–Ge(111) surfaces also contained no detectable contaminants (see Supporting Information).

Figure 4 also shows high-resolution XP spectra of the Ge 3d and Br 3d photoelectron regions taken at three points during the synthesis procedure: the hydrogen-terminated, bromine-terminated, and methyl-terminated Ge(111) surfaces. No oxidation of the underlying Ge, which would produce peaks shifted to higher binding energy (31–33 eV) than the bulk Ge $3d_{3/2}$ and $3d_{5/2}$ peaks, was detected in any of the Ge 3d spectra. The Br 3d XP spectra showed the appearance of Br $3d_{3/2}$ and $3d_{5/2}$ peaks upon 1 min reaction of H–Ge(111) in $CCl_3Br(l)$. No Br was detectable after subsequent methylation of the Br–Ge(111) surface in $(CH_3)_2Mg/THF/1,4$-dioxane. The bromine coverage for the Br–Ge(111) surface was estimated to be 0.74 ± 0.13 monolayers (ML; 1 ML = 1 adsorbed Br per surface Ge atom), and longer bromination times did not lead to an increase in coverage.

Figure 5 shows a representative high-resolution XP spectrum of the C 1s photoelectron region of a CH_3–Ge(111) surface, with the spectrum fit to five peaks. The largest peak was centered at 285.2 eV and is attributed to the C–C species associated with adventitious hydrocarbons. A small peak at
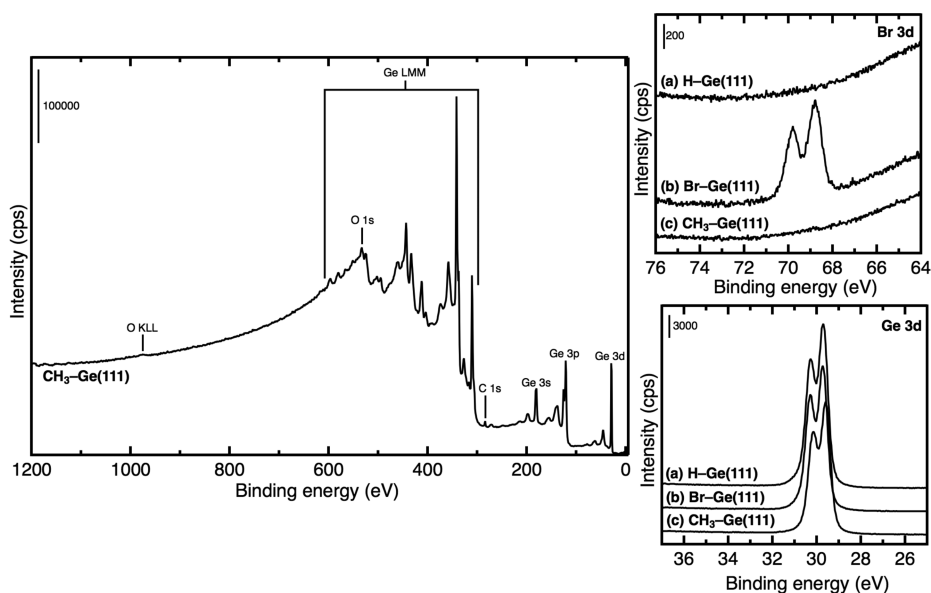
Figure 4. Left panel: XP survey spectrum of a CH$_3$−Ge(111) surface. Right panels: high-resolution XP spectra of the Br 3d (top) and Ge 3d (bottom) photoelectron regions of (a) an H−Ge(111) surface, (b) a Br−Ge(111) surface, and (c) a CH$_3$−Ge(111) surface.
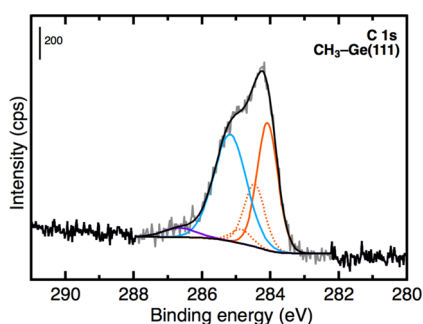

Figure 5. High-resolution XP spectrum of the C 1s photoelectron region of a CH$_3$−Ge(111) surface. As described in the text, the fitted peaks are assigned to C−O (purple), C−C (blue), C−Ge (solid orange), and C−Ge with vibrational losses (dotted orange).

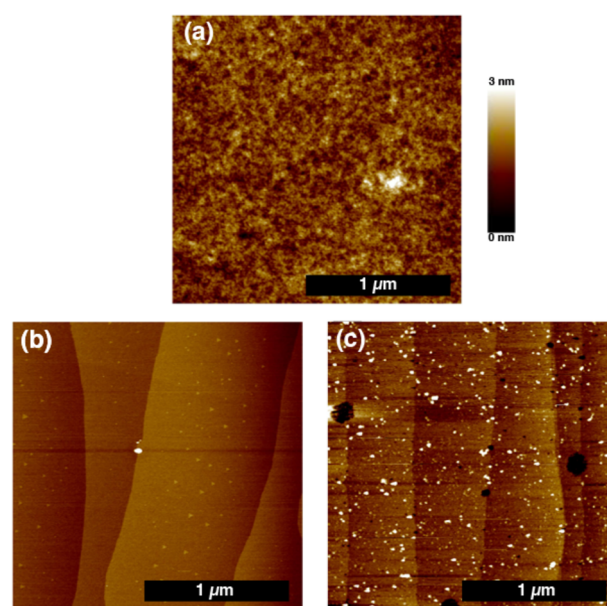**Figure 6.** Representative atomic-force micrographs of (a) an HF-etched Ge(111) surface, (b) an H−Ge(111) surface prepared by annealing under H$_2$(g), and (c) a CH$_3$−Ge(111) surface.

higher binding energy (286.7 eV) can be attributed to C−O species in oxygen-containing adventitious hydrocarbons. The peak at 284.1 eV can be attributed to C−Ge from methyl groups covalently bonded to the Ge surface, similar to previous reports for CH$_3$−Ge(111) and CH$_3$−Si(111) surfaces.[7,21] In addition, to account for the vibrational fine structure, peaks were fit at fixed energy (+0.38, +0.76 eV) and relative area (49%, 11%) compared to the main C−Ge peak; these vibrational loss peaks are shown by the dotted peaks in Figure 5. The vibrational fine structure has been shown to produce an asymmetric peak shape for CH$_3$−Si(111) surfaces,[21] and the same peak shape was found to provide the best fit for as-prepared CH$_3$−Ge(111) surfaces as well as for CH$_3$−Ge(111) surfaces that had been annealed to remove adventitious hydrocarbons (vide infra). The methyl surface coverage was estimated to be 0.80 ± 0.02 ML (1 ML = 1 methyl group per surface Ge atom) using the substrate-overlayer model (eq 1) or 0.83 ± 0.03 ML by comparison to reference CH$_3$−Si(111) surfaces (eq 3). No Br was detected by XPS (Figure 4).

C. Surface Imaging. Figure 6 presents atomic-force micrographs of an HF-etched Ge(111) surface, an H−Ge(111) surface after annealing under H$_2$(g), and a CH$_3$−Ge(111) surface. After etching in HF (Figure 6a), the surface

exhibited nanometer-scale roughness. Annealing under H$_2$(g) removed this roughness, and similar to previous reports, a terraced surface with terrace widths on the order of hundreds of microns was produced.[22−24] The terraces were atomically flat, aside from small raised triangular protrusions that were attributed to raised (111) facets. The step height between terraces, as determined by averaging several measurements from Figure 6b, was 318 ± 12 pm, in close agreement with the 327 pm (111) interplanar spacing calculated on the basis of the lattice parameter of Ge (565.8 pm[25]). The surface structure was mostly unchanged by methylation in (CH$_3$)$_2$Mg/THF/1,4-dioxane (Figure 6c), aside from the appearance of small particles and etch pits. The terraced structure remained intact,

with similar step heights to those observed for the H−Ge(111) surface.

Figure 7 shows representative EC-STM images of a CH_3−Ge(111) surface. The 500 × 500 nm^2 image (Figure 7a)
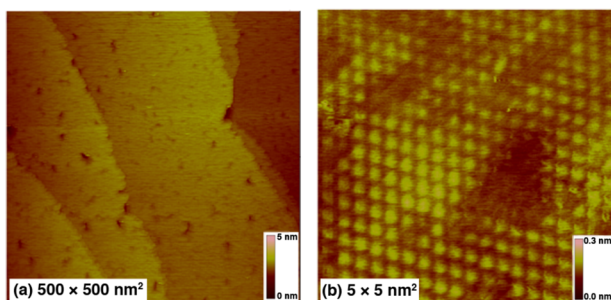

Figure 7. EC-STM images of a CH_3−Ge(111) surface: (a) 500 × 500 nm^2 area collected at the open-circuit potential with −500 mV bias voltage and 2 nA tunneling current, (b) 5 × 5 nm^2 area collected at the open-circuit potential with −300 mV bias voltage and 5 nA tunneling current.

showed a terraced surface, similar to the AFM image in Figure 6c. The terrace step height was measured to be 320 ± 20 pm, in agreement with the AFM data. Figure 7b shows a high-resolution EC-STM image of a 5 × 5 nm^2 area of a CH_3−Ge(111) surface. The data showed an array of bright protrusions, which are assigned to individual surface-bound methyl groups. The distance between neighboring (methyl group) bright spots was measured to be 380 ± 20 pm, which is in agreement with the distance between neighboring Ge atoms on an unreconstructed Ge(111) surface (400 pm based on a lattice parameter of 565.8 pm) considering that some drift was observed during collection of EC-STM images. Thus, the pattern of EC-STM bright spots associated with methyl groups is consistent with methylation of the atop Ge(111)-(1 × 1) sites. The dark spots in both EC-STM images likely represent surface sites that had not been terminated with methyl groups, and these sites may be bare Ge, oxidized Ge, H-terminated Ge, or Ge atoms terminated by other species. The methyl surface coverage in the area imaged in Figure 7b was 0.85−0.90 ML.

D. Low-Energy Electron Diffraction. Figure 8 shows the LEED patterns, at three different primary electron energies,
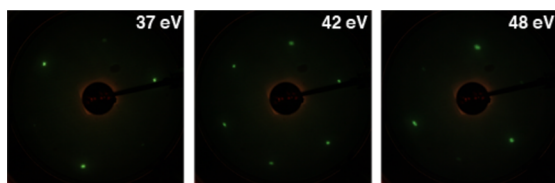

Figure 8. LEED patterns of a CH_3−Ge(111) surface recorded at primary electron energies of 37, 42, and 48 eV, respectively.

obtained from a CH_3−Ge(111) surface. Relatively low primary electron energies (37−48 eV) were used to minimize the electron escape depth. Patterns with a 3-fold symmetry were observed, consistent with a 1 × 1 structure. The sharp, bright diffraction spots and low background intensity indicated that the surface was well-ordered, and were consistent with the large, atomically flat terraces observed by AFM. The observed LEED patterns indicate that the Ge(111) surface is unreconstructed and well-ordered, but the LEED patterns do

not necessarily provide direct information regarding the ordering and symmetry of the methyl overlayer, as the thin organic layer may have a low cross section for scattering low-energy electrons. The energy dependence of the LEED pattern was analogous to LEED data on CH_3− and C_2H_5−Si(111) surfaces.[21,26]

E. Thermal Stability in UHV. Figure 9 shows the high-resolution C 1s XP spectra of a CH_3−Ge(111) surface as-
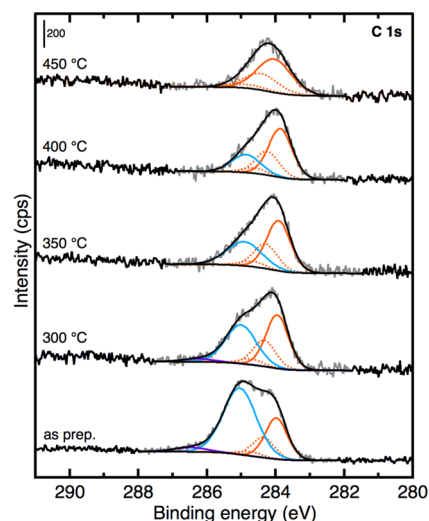

Figure 9. High-resolution XP spectra of the C 1s photoelectron region of a CH_3−Ge(111) surface (bottom to top) as-prepared and after sequential 60 min anneals in UHV at 300, 350, 400, and 450 °C, respectively. As described in the text, the fitted peaks are assigned to C−O (purple), C−C (blue), C−Ge (solid orange), and C−Ge with vibrational losses (dotted orange).

prepared and after annealing in UHV for 60 min at 300, 350, 400, and 450 °C, respectively. Annealing up to 400 °C resulted in a reduction in the peaks attributed to adventitious C−C and C−O species, with negligible change in the position or area of the C−Ge peak. Upon annealing to 450 °C, several experiments showed that the area of the C−Ge peak had been reduced, indicating the loss of methyl carbon from the surface. In addition, the C−Ge peak broadened and shifted ∼0.2 eV higher in binding energy after annealing to 450 °C, suggesting a chemical change of some or all of the surface-bound methyl groups. Even when little or no adventitious carbon remained after annealing, the C 1s data were best fit by including the vibrational fine structure peaks, supporting the use of this fitting method. No change was observed in the Ge 3d XP spectrum throughout the annealing process (see Supporting Information).

F. Surface Oxidation. Figure 10 shows high-resolution Ge 3d XP spectra of an H−Ge(111) surface and of a CH_3−Ge(111) surface, upon exposure to ambient laboratory air. Under such conditions, the H−Ge(111) surface oxidized on a time scale of hours, as indicated by the appearance of a peak at 32.5−33.3 eV, corresponding to GeO_2. The CH_3−Ge(111) surface also oxidized in air, but at a much slower rate than the H−Ge(111) surface. The difference in oxidation rates between the H−Ge(111) and CH_3−Ge(111) surfaces is depicted in Figure 10c, which shows the oxide coverage in ML calculated using eq 4. After 134 h in air, the H−Ge(111) surface contained 1.15 ML of oxide, whereas the CH_3−Ge(111) surface contained 0.12 ML of oxide after 432 h in air.
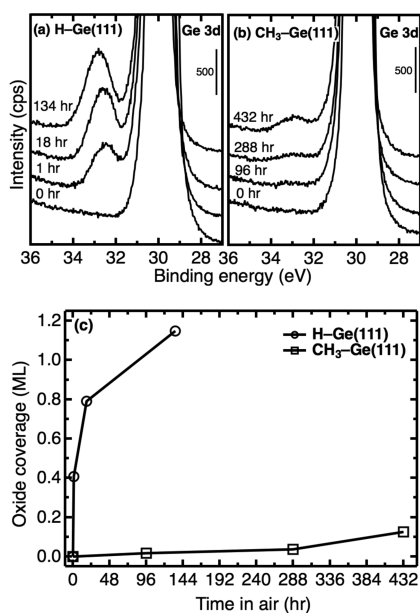
Figure 10. High-resolution XP spectra of the Ge 3d photoelectron region of (a) an H–Ge(111) surface and (b) a CH₃–Ge(111) surface exposed to ambient laboratory air for varying amounts of time and (c) the calculated oxide coverages of both surfaces as a function of time exposed to air.

◼ DISCUSSION

A. Hydrogen Termination. The presence of Ge–H stretching and deformation modes in the FTIR spectra of Ge(111) annealed under H₂ at 850 °C (Figure 1a,b) is consistent with the formation of a H-terminated Ge surface. The angular dependence of these vibrational modes indicates that the ν(Ge–H) and δ(Ge–H) modes are primarily polarized perpendicular and parallel to the surface, respectively, which is consistent with the Ge–H bond being oriented perpendicular to the surface. The sharpness and polarization of the ν(Ge–H) and δ(Ge–H) peaks, the absence of vibrations associated with GeH₂ or GeH₃, and the absence of detectable contaminants by XPS, all suggest that the H–Ge(111) surface formed by this procedure is chemically analogous to that formed by NH₄F etching of Si(111),[27] and that such surfaces consist of H atoms bonded directly on atop surface Ge atoms. In addition, AFM micrographs of the H–Ge(111) surface (Figure 6b) showed atomically flat terraces separated by monatomic steps, similar to what has been observed for Si(111) surfaces etched by NH₄F(aq).[28] Building on previous work demonstrating formation of atomically flat Ge(111) by annealing in H₂,[22–24] the data presented here demonstrates that the resulting surface is characterized by a highly homogeneous Ge–H surface termination.

B. Bromine Termination. Bromination of the H–Ge(111) surface was achieved by reaction in CCl₃Br, as has been done for Si(111) surfaces.[29] The appearance of Br 3d photoelectron peaks in the XP spectrum of Br–Ge(111) (Figure 4) provides evidence for bromination of the Ge by this reaction sequence. The Br coverage estimated from the XPS data (0.74 ± 0.13 ML), and the lack of observable ν(Ge–H) and δ(Ge–H) peaks in the FTIR spectrum of the Br–Ge(111) surface (Figure 1c), suggest that, upon bromination, Ge–H surface species were essentially completely replaced by Ge–Br species. Bromination in CCl₃Br was chosen over other halogenation methods because the CCl₃Br reagent did not result in significant etching of the Ge(111) surface.

C. Methyl Termination. The formation of a methyl-functionalized Ge(111) surface was demonstrated by FTIR spectroscopy, HREELS, and XPS. The FTIR and HREEL spectra of CH₃–Ge(111) exhibited ν(C–H), δ_s(CH₃), δ_a(CH₃), and ρ(CH₃) modes at similar frequencies to those reported for methyl-terminated Ge(111) and Si(111) surfaces[8,30] as well as at frequencies similar to those typically observed for Ge–CH₃-containing organometallic compounds.[31] The angular dependence of the δ_s(CH₃) and ρ(CH₃) modes in the FTIR spectra (Figure 2) is consistent with the Ge–C bond being oriented perpendicular to the surface. The HREELS peak at 568 cm⁻¹ (Figure 3) provides direct evidence for the formation of a covalent Ge–C bond. For comparison, the Si–C stretching mode of CH₃–Si(111) surfaces occurs at 678–683 cm⁻¹.[32–35] Assuming a harmonic oscillator model and considering the observed ν(Ge–H) frequency in conjunction with the reduced masses of Ge–H versus Ge–CH₃, the ν(Ge–C) mode is thus predicted to appear at 556 cm⁻¹, in close agreement with the observed peak at 568 cm⁻¹. In addition, the observed 568 cm⁻¹ peak lies within the 535–641 cm⁻¹ range typical of Ge–C stretching modes in organometallic compounds that contain Ge–CH₃ groups.[31] Future work will compare the experimentally observed vibrational frequencies to frequencies predicted by theoretical calculations of a CH₃–Ge(111) surface.[36] Together, these data from vibrational spectroscopy provide evidence for covalent functionalization of the Ge(111) surface with methyl groups situated directly atop surface Ge atoms, to yield a Ge–C bond perpendicular to the surface.

The presence of a peak at 284.1 eV in the C 1s XP spectrum (Figure 5) of the surface reacted with (CH₃)₂Mg is also consistent with covalent functionalization of the surface with methyl groups. Due to the lower electronegativity of Ge than C, C covalently bonded to Ge is expected to have a lower C 1s binding energy than C bonded to C in adventitious carbon. Consistently, a C 1s peak at ~284 eV has been attributed to the C–Ge and C–Si species of alkylated Ge(111) and Si(111) surfaces, respectively.[7,21,26,37,38] Additional evidence that the C 1s photoelectron peak at 284.1 eV corresponds to covalently bonded C–Ge is provided by the XPS data on annealed surfaces (Figure 9). Annealing to 400 °C led to no significant change in the area of the C–Ge peak. Annealing to 450 °C led to a reduction in the C–Ge peak area along with a small broadening and shift (+0.2 eV) of the C–Ge peak (Figure 9) and no significant change of the Ge 3d peaks (Supporting Information Figure S3), suggesting that the methyl group desorbed from the surface or otherwise underwent a chemical transformation on the surface. These data indicate a thermal stability limit of the CH₃–Si(111) surface of ~400 °C, similar to the ~440 °C measured for a CH₃–Si(111) surface.[26] The 450 °C anneal led to a reduction in the C–Ge peak area without a significant change in either the C 1s (Figure 9) or Ge 3d peaks (Supporting Information Figure S3), suggesting that the methyl group desorbed from the surface at this temperature rather than incorporating into the bulk. Annealing to 400 °C removed essentially all physisorbed adventitious hydrocarbons, as evidenced by the disappearance of the C 1s peaks at 285.2 and 286.7 eV, respectively. These data indicate that the C 1s peak at 284.1 eV corresponds to a carbon species strongly bound to the surface, consistent with the assignment of this

signal to C—Ge associated with covalently bound methyl groups.

Two of the defining features of methyl-terminated Si(111) surfaces are the essentially 100% coverage of surface Si atoms achieved and the chemical passivation afforded by the methyl overlayer.[39] Using the area of the C 1s photoelectron peak at 284.1 eV assigned to C—Ge, the coverage of CH$_3$—Ge(111) surfaces was estimated to be 0.80 ± 0.02 ML (substrate-overlayer model) or 0.83 ± 0.03 ML (comparison to CH$_3$—Si(111) surface). It should be noted that both models rely on the accuracy of a number of parameters that are not easily measured. However, XPS data showed no residual Br, no measurable oxidation immediately after synthesis, and no other contaminant elements; and FTIR spectroscopy showed no measurable Ge—H stretching or bending. By ruling out other likely surface species, these data suggest that the surface coverage of methyl groups may, in fact, be closer to 1 ML than indicated by XPS coverage estimates. In fact, the EC-STM images (Figure 7) provided direct, compelling evidence that the methyl surface coverage is closer to 100% than estimated from XPS data. Specifically, the high-resolution EC-STM image of Figure 7b shows that the methyl groups formed an ordered array with spacing that matched that of surface atoms on an unreconstructed Ge(111) surface, with the large area image (Figure 7a) showing relatively few defects over a 500 × 500 nm^2 area. In addition, relatively high count rates have been observed for helium-atom scattering off of CH$_3$—Ge(111) surfaces prepared by the method described here, suggesting that these surfaces have relatively low defect densities.[36]

Methyl termination of Ge(111) also produced a significantly improved resistance to oxidation in air as compared to an H—Ge(111) surface (Figure 10). A H—Ge(111) surface contained 0.41 ML of oxide after 1 h of air exposure and contained 1.15 ML of oxide after 134 h of air exposure. In contrast, a CH$_3$—Ge(111) surface contained only 0.12 ML of oxide after 432 h of air exposure. In fact, the CH$_3$—Ge(111) surface exhibited even greater oxidation resistance than CH$_3$—Si(111) surfaces. A CH$_3$—Si(111) surface was reported to contain 0.8 ± 0.4 ML of oxide after 216 h in air[40] compared to 0.03 ML oxide after 288 h in air measured for CH$_3$—Ge(111).

Previous studies of Ge methylation used wet-chemical functionalization methods, which resulted in atomically rough surfaces.[7,8,11] In contrast, the method described herein enabled the formation of H—Ge(111) surfaces with atomically flat terraces (Figure 6b). Moreover, annealing in H$_2$(g) yielded a very homogeneous and well-defined monohydride surface without detectable di- or trihydride surface species. The AFM images after methylation (Figure 6c), and the sharp, bright 1 × 1 diffraction spots observed by LEED of CH$_3$—Ge(111) surfaces (Figure 8), indicated that the surface structure remained atomically flat and a highly homogeneous (111)-(1 × 1) structure was preserved upon methylation. This conclusion is further supported by the high-resolution EC-STM image in Figure 7b, which shows bright protrusions assigned to methyl groups in a (111)-(1 × 1) array with a spacing commensurate with that of atop Ge atoms on an unreconstructed Ge(111) surface. The appearance of pits in the atomic-force and EC-STM micrographs of the CH$_3$—Ge(111) surface suggests that the methylation step slowly etched the surface; however, most of the surface remained terraced and atomically flat. Given that the Ge lattice constant is only ~4% larger than that of Si, the atomically flat Ge(111) surface can be 100% terminated by closely packed methyl groups, in a similar fashion to what has been observed for CH$_3$—Si(111) by scanning-tunneling microscopy.[13]

CONCLUSIONS

Atomically flat Ge(111) surfaces were prepared by annealing in H$_2$(g), and FTIR spectroscopy confirmed that these surfaces were Ge—H terminated with the Ge—H bond oriented normal to the surface, with no detectable GeH$_2$ or GeH$_3$ surface species. Bromination of H—Ge(111) surfaces was achieved by reaction of H—Ge(111) in neat CCl$_3$Br. FTIR spectroscopy showed the complete removal of Ge—H species, and XPS data showed 0.74 ± 0.13 ML of Br on the surface. Atomically flat CH$_3$—Ge(111) surfaces were prepared by methylation of Br—Ge(111) surfaces in (CH$_3$)$_2$Mg. HREELS data provided evidence for the formation of a covalent Ge—C bond, and the dependence of the methyl umbrella and rocking IR absorptions on the incident light angle indicated that methyl groups were oriented such that the Ge—C bond was normal to the surface. AFM and EC-STM images of the CH$_3$—Ge(111) surface showed that the surface remained mostly terraced and atomically flat, and LEED images showed sharp, bright diffraction spots with 3-fold symmetry indicating a highly ordered unreconstructed surface. EC-STM also confirmed that methyl groups form an ordered array with spacing equal to that of a Ge(111)-(1 × 1) surface. XP spectra contained a low binding-energy C 1s peak that remained unchanged upon annealing to 400 °C, consistent with formation of a C—Ge covalent bond. The surface coverage calculated based on the area of this peak was estimated from XPS data to be 0.80–0.83 ML, but EC-STM data indicated that the surface coverage is closer to a complete monolayer with few defects. No surface oxidation was detected immediately after preparation of the CH$_3$—Ge(111) surfaces, and the methyl-terminated surface exhibited significantly greater resistance to oxidation in air than a hydrogen-terminated Ge(111) surface.

ASSOCIATED CONTENT

Ⓢ Supporting Information

Mg 2s XP spectrum of a CH$_3$—Ge(111) surface, XP survey spectra of H—Ge(111) and Br—Ge(111) surfaces, and Ge 3d XP spectra of a CH$_3$—Ge(111) surface after annealing. The Supporting Information is available free of charge on the ACS Publications website at DOI: 10.1021/jacs.5b03339.

AUTHOR INFORMATION

Corresponding Author
*E-mail: nslewis@caltech.edu.

Notes
The authors declare no competing financial interest.

ACKNOWLEDGMENTS

■ REFERENCES

(1) Frank, M. M.; Koester, S. J.; Copel, M.; Ott, J. A.; Paruchuri, V. K.; Shang, H.; Loesing, R. *Appl. Phys. Lett.* **2006**, *89*, 112905−112903.

(2) Brunco, D. P.; De Jaeger, B.; Eneman, G.; Mitard, J.; Hellings, G.; Satta, A.; Terzieva, V.; Souriau, L.; Leys, F. E.; Pourtois, G.; Houssa, M.; Winderickx, G.; Vrancken, E.; Sioncke, S.; Opsomer, K.; Nicholas, G.; Caymax, M.; Stesmans, A.; Van Steenbergen, J.; Mertens, P. W.; Meuris, M.; Heyns, M. M. *J. Electrochem. Soc.* **2008**, *155*, H552−H561.

(3) Takagi, S.; Tezuka, T.; Irisawa, T.; Nakaharai, S.; Maeda, T.; Numata, T.; Ikeda, K.; Sugiyama, N. *Mater. Sci. Eng., B* **2006**, *135*, 250−255.

(4) King, R. R.; Law, D. C.; Edmondson, K. M.; Fetzer, C. M.; Kinsey, G. S.; Yoon, H.; Sherif, R. A.; Karam, N. H. *Appl. Phys. Lett.* **2007**, *90*, 183516.

(5) Guter, W.; Schöne, J.; Philipps, S. P.; Steiner, M.; Siefer, G.; Wekkeli, A.; Welser, E.; Oliva, E.; Bett, A. W.; Dimroth, F. *Appl. Phys. Lett.* **2009**, *94*, 223504.

(6) Loscutoff, P. W.; Bent, S. F. *Annu. Rev. Phys. Chem.* **2006**, *57*, 467−495.

(7) Knapp, D.; Brunschwig, B. S.; Lewis, N. S. *J. Phys. Chem. C* **2010**, *114*, 12300−12307.

(8) Knapp, D.; Brunschwig, B. S.; Lewis, N. S. *J. Phys. Chem. C* **2011**, *115*, 16389−16397.

(9) Bansal, A.; Li, X.; Lauermann, I.; Lewis, N. S.; Yi, S. I.; Weinberg, W. H. *J. Am. Chem. Soc.* **1996**, *118*, 7225−7226.

(10) Haber, J. A.; Lewis, N. S. *J. Phys. Chem. B* **2002**, *106*, 3639−3656.

(11) Knapp, D. Chemistry and Electronics of the Ge(111) Surface, Ph.D. Thesis, California Institute of Technology, 2011.

(12) Webb, L. J.; Nemanick, E. J.; Biteen, J. S.; Knapp, D. W.; Michalak, D. J.; Traub, M. C.; Chan, A. S. Y.; Brunschwig, B. S.; Lewis, N. S. *J. Phys. Chem. B* **2005**, *109*, 3930−3937.

(13) Yu, H.; Webb, L. J.; Ries, R. S.; Solares, S. D.; Goddard, W. A.; Heath, J. R.; Lewis, N. S. *J. Phys. Chem. B* **2005**, *109*, 671−674.

(14) Niwa, D.; Inoue, T.; Fukunaga, H.; Akasaka, T.; Yamada, T.; Homma, T.; Osaka, T. *Chem. Lett.* **2004**, *33*, 284−285.

(15) Becker, J. S.; Brown, R. D.; Johansson, E.; Lewis, N. S.; Sibener, S. J. *J. Chem. Phys.* **2010**, *133*, 104705.

(16) Deegan, T.; Hughes, G. *Appl. Surf. Sci.* **1998**, *123−124*, 66−70.

(17) Kato, K.; Sakashita, M.; Takeuchi, W.; Nakatsuka, O.; Zaima, S. *J. Phys.: Conf. Ser.* **2013**, *417*, 012001.

(18) Rivillon, S.; Chabal, Y. J.; Amy, F.; Kahn, A. *Appl. Phys. Lett.* **2005**, *87*, 253101−253103.

(19) Lu, G.; Crowell, J. E. *J. Chem. Phys.* **1993**, *98*, 3415−3421.

(20) Soriaga, M. P.; Chen, X.; Li, D.; Stickney, J. L. High Resolution Electron Energy-Loss Spectroscopy. *Encyclopedia of Inorganic Chemistry*; John Wiley & Sons, Ltd: New York, 2006, 1−18.

(21) Hunger, R.; Fritsche, R.; Jaeckel, B.; Jaegermann, W.; Webb, L. J.; Lewis, N. S. *Phys. Rev. B* **2005**, *72*, 045317.

(22) Nishimura, T.; Kabuyanagi, S.; Zhang, W.; Lee, C. H.; Yajima, T.; Nagashio, K.; Toriumi, A. *Appl. Phys. Express* **2014**, *7*, 051301.

(23) Nishimura, T.; Kabuyanagi, S.; Lee, C.; Yajima, T.; Nagashio, K.; Toriumi, A. *ECS Trans.* **2013**, *58*, 201−206.

(24) Nishimura, T.; Lee, C. H.; Nagashio, K.; Akira, T.; Step. *Appl. Phys. Express* **2012**, *5*, 121301.

(25) Straumanis, M. E.; Aka, E. Z. *J. Appl. Phys.* **1952**, *23*, 330−334.

(26) Jaeckel, B.; Hunger, R.; Webb, L. J.; Jaegermann, W.; Lewis, N. S. *J. Phys. Chem. C* **2007**, *111*, 18204−18213.

(27) Higashi, G. S.; Chabal, Y. J.; Trucks, G. W.; Raghavachari, K. *Appl. Phys. Lett.* **1990**, *56*, 656−658.

(28) Higashi, G. S.; Becker, R. S.; Chabal, Y. J.; Becker, A. J. *Appl. Phys. Lett.* **1991**, *58*, 1656−1658.

(29) He, J.; Patitsas, S. N.; Preston, K. F.; Wolkow, R. A.; Wayner, D. D. M. *Chem. Phys. Lett.* **1998**, *286*, 508−514.

(30) Webb, L. J.; Rivillon, S.; Michalak, D. J.; Chabal, Y. J.; Lewis, N. S. *J. Phys. Chem. B* **2006**, *110*, 7349−7356.

(31) Mehrotra, R. C. *Organometallic Chemistry*; New Age International (P) Limited: New Delhi, India, 2007.

(32) Yamada, T.; Kawai, M.; Wawro, A.; Suto, S.; Kasuya, A. *J. Chem. Phys.* **2004**, *121*, 10660−10667.

(33) Yamada, T.; Inoue, T.; Yamada, K.; Takano, N.; Osaka, T.; Harada, H.; Nishiyama, K.; Taniguchi, I. *J. Am. Chem. Soc.* **2003**, *125*, 8039−8042.

(34) Johansson, E.; Hurley, P. T.; Brunschwig, B. S.; Lewis, N. S. *J. Phys. Chem. C* **2009**, *113*, 15239−15245.

(35) Amy, S. R.; Michalak, D. J.; Chabal, Y. J.; Wielunski, L.; Hurley, P. T.; Lewis, N. S. *J. Phys. Chem. C* **2007**, *111*, 13053−13061.

(36) Hund, Z. M.; Nihill, K. J.; Campi, D.; Wong, K. T.; Lewis, N. S.; Bernasconi, M.; Benedek, G.; Sibener, S. J. Atomic Surface Structure of CH_3-Ge(111) Characterized by Helium Atom Diffraction and Density Functional Theory, submitted.

(37) Nemanick, E. J.; Hurley, P. T.; Brunschwig, B. S.; Lewis, N. S. *J. Phys. Chem. B* **2006**, *110*, 14800−14808.

(38) Plass, K. E.; Liu, X.; Brunschwig, B. S.; Lewis, N. S. *Chem. Mater.* **2008**, *20*, 2228−2233.

(39) Wong, K. T.; Lewis, N. S. *Acc. Chem. Res.* **2014**, *47*, 3037−3044.

(40) Webb, L. J.; Lewis, N. S. *J. Phys. Chem. B* **2003**, *107*, 5404−5412.